

# Uncertainty estimates for the FAPAR operational products derived from MERIS — Impact of top-of-atmosphere radiance uncertainties and validation with field data

Nadine Gobron<sup>a,\*</sup>, Bernard Pinty<sup>a</sup>, Ophélie Aussedat<sup>a</sup>, Malcolm Taberner<sup>a</sup>, Olga Faber<sup>b</sup>, Frédéric Mélin<sup>a</sup>, Thomas Lavergne<sup>a</sup>, Monica Robustelli<sup>a</sup>, Paul Snoeij<sup>c</sup>

<sup>a</sup> European Commission - DG Joint Research Centre, Institute for Environment and Sustainability, Global Environment Monitoring Unit, TP 440, via E. Fermi, 21020 Ispra(VA), Italy

<sup>b</sup> Carsten Brockmann Consult, Ottilie-Baader-Str. 15, 21035 Hamburg, Germany

<sup>c</sup> European Space Agency EOP-SMS European Space Research and Technology Centre -, Keplerlaan 1, P.O. Box 299, 2200 AG Noordwijk, The Netherlands

Received 20 March 2007; received in revised form 14 September 2007; accepted 15 September 2007

## Abstract

This paper discusses the accuracy of the operational Medium Resolution Imaging Spectrometer (MERIS) Level 2 land product which corresponds to the Fraction of Absorbed Photosynthetically Active Radiation (FAPAR). The FAPAR value is estimated from daily MERIS spectral measurements acquired at the top-of-atmosphere, using a physically based approach. The products are operationally available at the reduced spatial resolution, *i.e.* 1.2 km, and can be computed at the full spatial resolution, *i.e.* at 300 m, from the top-of-atmosphere MERIS data by using the same algorithm. The quality assessment of the MERIS FAPAR products capitalizes on the availability of five years of data acquired globally. The actual validation exercise is performed in two steps including, first, an analysis of the accuracy of the FAPAR algorithm itself with respect to the spectral measurements uncertainties and, second, with a direct comparison of the FAPAR time series against ground-based estimations as well as similar FAPAR products derived from other optical sensor data. The results indicate that the impact of top-of-atmosphere radiance uncertainties on the operational MERIS FAPAR products accuracy is expected to be at about 5–10% and the agreement with the ground-based estimates over different canopy types is achieved within  $\pm 0.1$ .

© 2007 Elsevier Inc. All rights reserved.

**Keywords:** FAPAR; FIPAR; Land surface; MERIS; MODIS; SeaWiFS; Remote sensing; Radiative transfer modeling; Validation

## 1. Introduction

Understanding the degree of climate change impacts on Earth system requires a better quantification of the uncertainties of the current terrestrial biosphere model outputs, which are mainly used for evaluating the carbon flux variations between land ecosystems and atmosphere. The geophysical products estimated from space remote sensing measurements can be used

directly or in data assimilation systems to better quantify this level of uncertainty (Knorr et al., 1995; Pinty et al., 2006a; Raupach et al., 2005; Rayner et al., 2005).

The validation of these biophysical products, mainly derived from optical sensors, is therefore highly desirable in order to evaluate whether the quality of the products is in conformity with the pre-flight specified accuracy that was imposed by the requirements of the anticipated application. The use of space derived products is moreover relevant for environmental applications at global scale only if long term time series of geophysical products are available: this calls for the use and

\* Corresponding author.

E-mail address: [Nadine.Gobron@jrc.it](mailto:Nadine.Gobron@jrc.it) (N. Gobron).

interpretation of the spectral measurements collected by multiple space sensors (these instruments may be either flying simultaneously or simply follow each other for recording spectral data over a long time period). The definition of the retrieval algorithm performance and actual validation exercises are required to assess the uncertainties required by any assimilation system dealing with global issues (GCOS, 2004; GTOS, 2006; GOOS, 2006). In addition, these analyses are a pre-requisite to merge biophysical products from various sensors, like for the sea surface temperature (Reynolds & Smith, 1994), the ocean color (Maritorea & Siegel, 2005; Mélin & Zibordi, 2007), the surface albedo using geostationary instruments (Govaerts et al., 2004) and the Fraction of Absorbed Photosynthetically Active Radiation (FAPAR) products.

Among the land geophysical products, both the surface albedo and FAPAR have been recognized to be essential variables in the climate system as well as for modeling the carbon cycle. The FAPAR products, directly linked to the photosynthesis process into vegetation canopies, can be either directly used as inputs into diagnostic biosphere models (Prince, 1991; Sellers et al., 1992; Knorr & Heimann, 1995; Running, 1986) or may serve as additional constraints during assimilation into more sophisticated schemes (Knorr et al., 1995, 2005b).

Further to the global climate change issues, this product is also a good indicator for assessing the changes of vegetation canopies state. Time series of these products can be analyzed for various regional land surface phenomena, like drought events or land degradation (Gobron et al., 2005a; Knorr et al., 2005a; Gobron et al., 2005b; Seiler & Csaplovics, 2005), or used for assessing environmental indicators such as the phenology parameters, like the growing season length (Verstraete et al., 2007) and more recently for the retrieval of radiation fluxes quantities for climate modeling (Pinty et al., 2006b). Of course, these applications are relevant only if the associated uncertainties are documented and provided which is hardly the case when empirical methods are used for trend analysis, as discussed in Hall et al. (2006).

Within the framework of delivering long time series of FAPAR products, Gobron et al. (2000, 2007) proposed a generic scheme from sensor specific algorithms that are devoted to the generation of equivalent, and thus comparable, FAPAR products derived from various optical sensors. This Joint Research Centre (JRC) FAPAR algorithm has been developed for the Medium Resolution Imaging Spectrometer (MERIS), Sea-viewing Wide Field-of-view Sensor (SeaWiFS) and MODerate Resolution Imaging Spectroradiometer (MODIS) (Gobron et al., 1999, 2001, 2006a, respectively) by using the measurements in the blue, red, and near-infrared spectral domains.

This manuscript focuses on the assessment of uncertainties of the operational MERIS FAPAR products, also called MERIS Global Vegetation Index (MGVI), available since the launch of the European Space Agency (ESA)'s Envisat platform in March 2002 at the reduced resolution, *i.e.* at 1.2 km spatial resolution. The data used are provided through the MERIS Catalogue and Inventory (MERCi) system for validation purposes (<http://merci-srv.eo.esa.int/merci/welcome.do>).

The first section presents an estimation of theoretical uncertainties with respect to the spectral measurements precision

that can be expected at the top-of-atmosphere (TOA) level in the three spectral domains. This propagation error analysis uses the derivative of the algorithm formulae with simulated Bidirectional Reflectance Factors (BRFs) TOA MERIS-like data as inputs with associated spectral band errors. This contribution thus complements previous efforts to document uncertainty estimates associated with the JRC FAPAR algorithm (Gobron et al., 2006b).

Since the FAPAR is a normalized radiant flux in the visible region of the solar spectrum, *i.e.* over the Photosynthetically Active Radiation (PAR) domain of (0.4–0.7  $\mu\text{m}$ ), the task of acquiring field measurements for validation exercises presents a range of challenges that vary in difficulty from one site to the other. Some of these difficulties for generating accurate ground-based estimations of FAPAR, particularly for the purpose of validating remote sensing products, are addressed in Gobron et al. (2006b) and are summarized at the beginning of the third section. This yields the categorization of ground-based FAPAR data sets according to their most probable radiative transfer (RT) regimes. The evaluation of the comparison results is indeed associated with the contextual difficulties specific to each site together with the corresponding in-situ data sets. The comparison results between remote sensing products from the MERIS instrument, but also from other sensors, and ground-based estimations of FAPAR are finally presented and analyzed.

## 2. Overview of the FAPAR algorithm and MERIS Level 2 products

The JRC generic FAPAR algorithm can be tailored to any sensor acquiring at least three narrow spectral bands in the blue, red and near-infrared regions of the solar spectrum. This algorithm capitalizes on the physics of remote sensing measurements and its development copes with the many operational constraints associated with the systematic processing and analysis of a large amount of data. Basically, the useful information on the presence and state of vegetation is derived from the red and the near-infrared spectral band measurements. The information contained in the blue spectral band, which is very sensitive to aerosol load, is ingested in order to account for atmospheric effects on these measurements. In the particular case of the MERIS sensor which was primarily designed for marine applications, the approach consists in analyzing the relationships between measurements in the blue spectral bands and those available in the red and near-infrared regions (e.g. Govaerts et al., 1999; Gobron et al., 1999). Such relationships can indeed be simulated for a variety of environmental conditions with RT models of the coupled vegetation-atmosphere system. The former are then exploited with polynomial expressions optimized in such a way that TOA BRF measurements in the blue are related to those taken at other spectral bands, located at longer wavelengths *e.g.*, in the red and near-infrared regions. This approach (called rectification) aims at decontaminating the BRFs from atmospheric effects without performing an explicit retrieval of the ambient atmospheric properties. The polynomial expressions are also built to simultaneously account for the dominant bidirectional effects. The latter are themselves approximated from an extensive set of one-

dimensional and/or three-dimensional RT simulations of the coupled surface-atmosphere system designed for mimicking typical vegetation canopy conditions (Gobron et al., 2000). This same training simulation set is then used to relate the radiative measurements from each typical vegetation canopy condition with their corresponding FAPAR values. In practice, the generic FAPAR algorithm thus implements a two step procedure where the spectral BRFs measured in the red and near-infrared bands are, first, rectified in order to ensure their optimal decontamination from atmospheric and angular effects and, second, combined together to estimate the FAPAR value. The most recent versions of the appropriate formulae and coefficients derived from the mathematical optimization are given in Gobron et al. (2002) for SeaWiFS, Gobron et al. (2007) for MERIS, and Gobron et al. (2006a) for MODIS, respectively.

Most results discussed in this paper are derived from the MERIS Level 2 products that have been processed by the operational software version IPF release 5.02 (Bourg & Obelensky, 2006). The actual reduced spatial resolution is at about 1.2 km and the following analysis has been conducted using data from the MERCI system. A long time series of equivalent products is also available using the SeaWiFS instrument resulting from a dedicated processing chain that was developed at JRC for delivering daily, 10-day and monthly time composite products at a global scale with spatial resolutions ranging from about 2 km up to 0.5 degrees (Mélin et al., 2002; Gobron et al., 2007). The JRC-FAPAR algorithm designed for MODIS data, which provides similar FAPAR products shown in this contribution, has been applied over various Earth Observation System (EOS) validation sites using the last available version of TOA radiances at 1.1 km, *i.e.* the MOD021KM products (Isaacman et al., 2003).

MERIS was launched on board the European platform Envisat and acquires operational data since mid 2002. MERIS scans the Earth's surface by the so called 'push-broom' method and the design is such that it can acquire data over the Earth whenever illumination conditions are suitable. However, the MGVI retrievals are considered valid only for sun zenith angle lower than 60°, a threshold set by the limitations of the RT model.

The instrument's 68.5° field-of-view around nadir covers a swath width of 1150 km and this wide field-of-view is shared between five identical optical modules arranged in a fan shape configuration. The accuracies of the spectral measurements of these five modules have been analysed by Delwart et al. (2003) for the calibration per se whereas Kneubuehler et al. (2004) and Govaerts and Clerici (2004), among others, performed vicarious calibration over land targets. The former concluded that the estimated radiometric uncertainty of MERIS bands was less than 4% with a degradation during 2 years of operations less than 3% in the blue bands (note that the operational data are corrected for this effect). The latter demonstrated that the performances of the MERIS bands are comparable to those of other instruments, like SeaWiFS or MODIS, between 2% – 4%.

Envisat has a repeat cycle of the reference orbit of 35 days and a specific geographical location can be seen by MERIS every three days, and 130 up to 205 measurements can be available during a full year over the validation sites used in this paper. This number of measurements, and associated FAPAR

estimates, decreases in the presence of clouds or cloud shadows.

### 3. Analysis of MGVI uncertainties

The results presented in this section are derived from the uncertainty analysis using the training simulation sets, *i.e.* MERIS simulated data already used in the development and the optimization of the retrieval algorithm itself. Each daily FAPAR value is computed through various polynomial formulae (see Gobron et al., 2007 for more details) using the BRFs measured at the TOA as input parameters. These formulae can therefore be mathematically derived to provide the uncertainties with respect to the BRF TOA,  $\rho_\lambda$ , in the three spectral bands ( $\lambda = \text{RED, BLUE and NIR}$ ), and their respective precision,  $\Delta\rho_\lambda$ .

$$\Delta\text{FAPAR} = \frac{\partial\text{FAPAR}}{\partial\rho_{\text{BLUE}}}\Delta\rho_{\text{BLUE}} + \frac{\partial\text{FAPAR}}{\partial\rho_{\text{RED}}}\Delta\rho_{\text{RED}} + \frac{\partial\text{FAPAR}}{\partial\rho_{\text{NIR}}}\Delta\rho_{\text{NIR}} \quad (1)$$

where  $\Delta\rho_\lambda$  are the uncertainties of TOA radiances for each spectral band  $\lambda$ . These uncertainties include various types of errors, like calibration precision or any instrumental error (note that we assume uncorrelated band to band uncertainties). The MERIS FAPAR products are operationally computed using the polynomial formula  $g_0$  which is a function of the two rectified channels,  $\rho_{\text{RectRED}}$  and  $\rho_{\text{RectNIR}}$ , in the red and near-infrared channel, respectively. Eq. (1) can be re-written as follows:

$$\Delta\text{FAPAR} = \frac{\partial g_0}{\partial\rho_{\text{RectRED}}}\Delta\rho_{\text{RectRED}} + \frac{\partial g_0}{\partial\rho_{\text{RectNIR}}}\Delta\rho_{\text{RectNIR}} \quad (2)$$

where the uncertainties in the red and near-infrared rectified channels are given by Eqs. (3) and (4), respectively.

$$\Delta\rho_{\text{RectRED}} = \frac{\partial g_1}{\partial\rho_{\text{BLUE}}}\Delta\rho_{\text{BLUE}} + \frac{\partial g_1}{\partial\rho_{\text{RED}}}\Delta\rho_{\text{RED}} \quad (3)$$

$$\Delta\rho_{\text{RectNIR}} = \frac{\partial g_2}{\partial\rho_{\text{BLUE}}}\Delta\rho_{\text{BLUE}} + \frac{\partial g_2}{\partial\rho_{\text{NIR}}}\Delta\rho_{\text{NIR}} \quad (4)$$

The mathematical formulae to evaluate the derivative of  $g_0$ , (polynomial formula to compute the FAPAR from the two rectified channels) with respect to the rectified red and near-infrared channels are given by Eqs. (7) and (8) in the Appendix. The derivatives of  $g_n$  (where  $g_n$  denotes  $g_1$  ( $g_2$ ) and corresponds to the polynomial formulae to compute the rectified channel in the red (near-infrared)) with respect to the blue band,  $\rho_{\text{BLUE}}$ , and with respect to the red (near-infrared) band,  $\rho_{\text{RED}}$  ( $\rho_{\text{NIR}}$ ), are also given in appendix by the Eqs. (9) and (10), respectively.

The BRF TOA simulated by the RT models, *i.e.* the semi-discrete model for the canopy layer (Gobron et al., 1997) and the Second Simulation of the Satellite Signal in the Solar Spectrum model (6S) for the atmosphere (Verote et al., 1997) are used to estimate the uncertainties of FAPAR with Eq. (1). The selected sample of state variables for the vegetated canopy includes two types of leaf angle distribution function (erectophile and planophile), five values of leaf area index (from 0.5 to 5.) and five values of albedo for the underneath soil (dark to

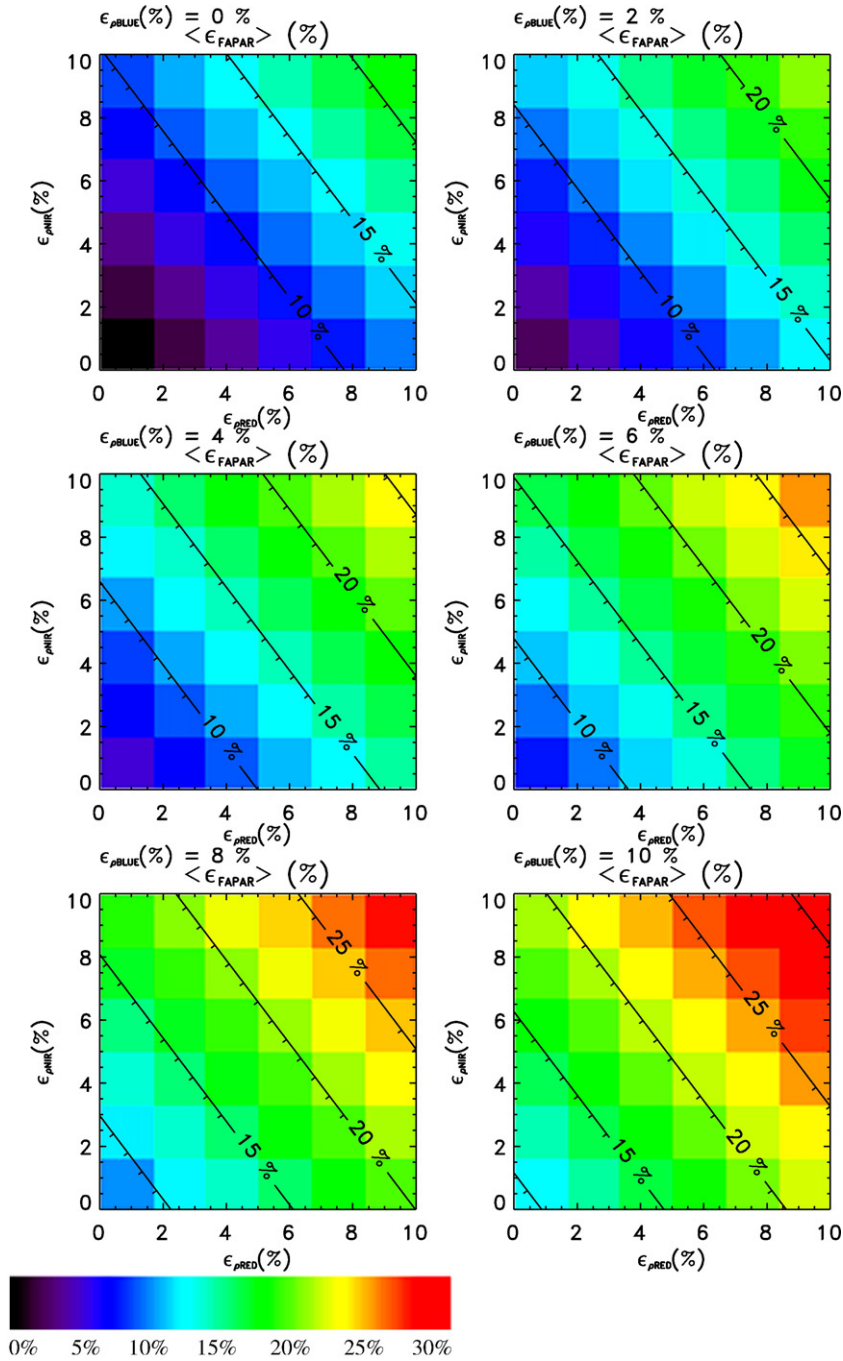


Fig. 1.  $\langle \epsilon_{FAPAR} \rangle$ , the averaged value over all uncertainty simulations, is mapped with respect to  $(\epsilon_{\rho_{RED}}, \epsilon_{\rho_{NIR}})$  for six values of  $\epsilon_{\rho_{BLUE}}$ .

bright). Two diameters of leaf, represented by a flat-disk, and two heights of canopy sample four types of dimensional and ‘architecture’ properties of the homogeneous canopy. The leaf spectral properties correspond to a standard green leaf. The FAPAR values computed with the semi-discrete model with this set of state variables range therefore between 0. to 0.99. The atmosphere layer properties are simulated using three values of aerosol optical thickness (*i.e.* 0.05, 0.3 and 0.8 at 550 nm) for a continental atmosphere type. Finally, two solar zenith angles, four viewing zenith angles and three azimuth angles encompass typical illumination and observation geometries. Using the

spectral properties of different instruments, *i.e.* spectral responses in the blue, red and near-infrared domains, the expected differences between JRC-FAPAR products derived from two sensors can also be simulated with respect to the so-called intercalibration differences.

### 3.1. Uncertainties of FAPAR with respect to MERIS spectral uncertainties

Fig. 1 illustrates the mean deviation,  $\langle \epsilon_{FAPAR} \rangle$ , defined as the averaged value of the relative deviation, *i.e.*  $\langle \frac{\Delta FAPAR}{FAPAR} \rangle$ , of all

simulated MERIS data, with respect to the spectral band uncertainties. Each panel exhibits the results corresponding to a given uncertainty value in the blue band,  $\varepsilon_{\rho_{\text{BLUE}}} = \frac{\Delta\rho_{\text{BLUE}}}{\rho_{\text{BLUE}}}$  indicated

in % above each panel. The values are mapped in the  $(\varepsilon_{\rho_{\text{RED}}}, \varepsilon_{\rho_{\text{NIR}}})$  plane with  $\varepsilon_{\rho_{\lambda}} = \frac{\Delta\rho_{\lambda}}{\rho_{\lambda}}$ . We can notice that the value of  $\langle \varepsilon_{\text{FAPAR}} \rangle$  increases as the spectral band uncertainties increase,

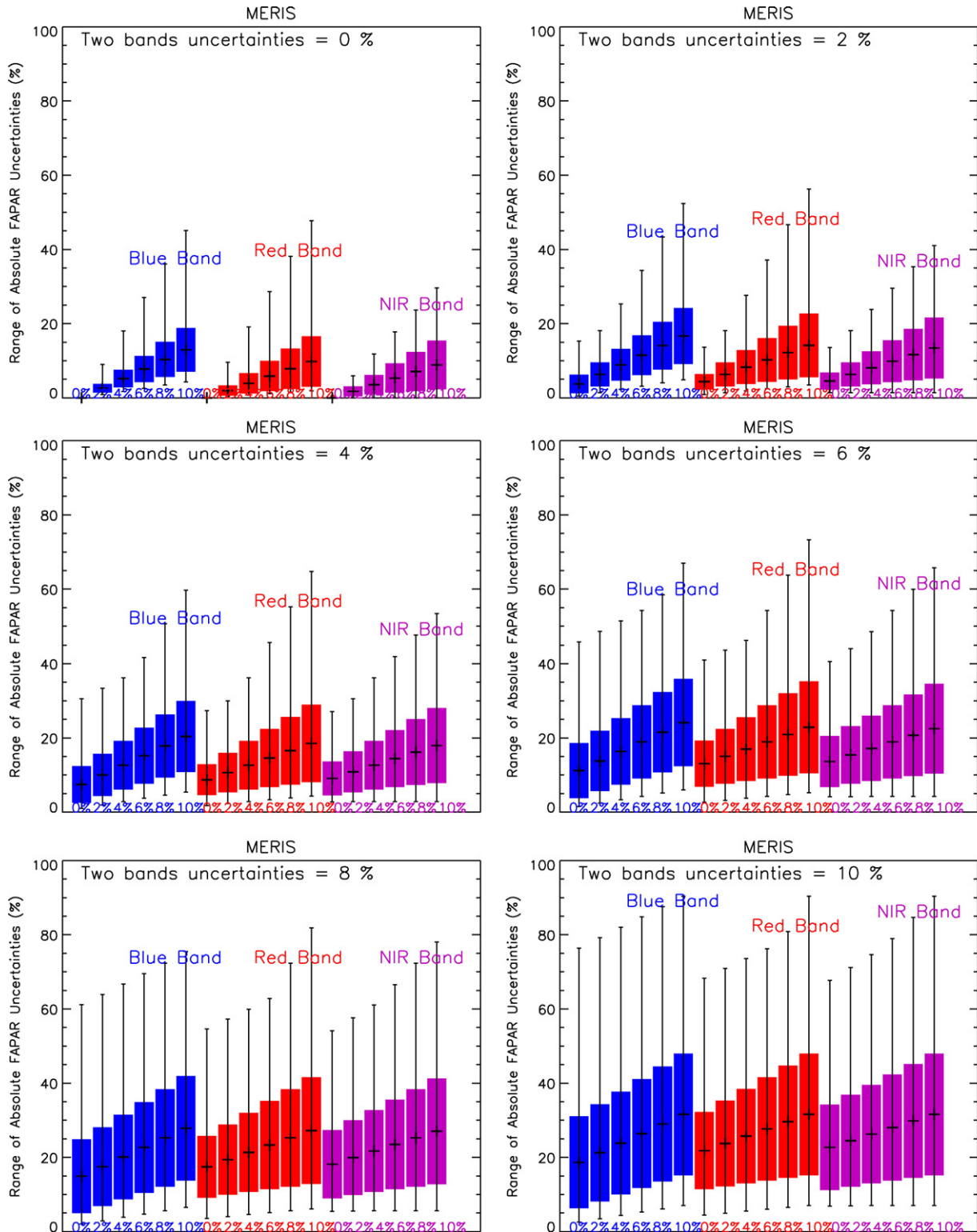


Fig. 2. The 6 panels illustrate how the range of deviation of FAPAR,  $\varepsilon_{\text{FAPAR}}$ , varies when the uncertainties of at least two bands of MERIS increase from 0% to 10% as function of the third uncertainty band in x-axis. The cross symbols correspond to averaged value of  $\varepsilon_{\text{FAPAR}}$  over all simulations with the standard deviation  $\pm\sigma$  in full column. Error bars indicate the minimum and maximum values in the ensemble.

mainly with the blue band. Among all the results, however, large variations occur and depend on the canopy type as well as on the atmospheric conditions and angular situations. These variations are illustrated by the panels of Fig. 2 which show the range of  $\varepsilon_{\text{FAPAR}}$  when the uncertainties of at least two bands of MERIS increase from 0% to 10% as function of the third band uncertainty (each of the 6 panels corresponds to 6 different values of uncertainty). The top left panel, for example, illustrates the variations of  $\varepsilon_{\text{FAPAR}}$  with respect to the uncertainties of the blue band (blue color bar), the red band (red color bar) and the near-infrared band (purple color bar), respectively for consistency with legend, assuming that the two other signals are ‘perfect’, i.e. with  $\varepsilon_{\rho\lambda}=0$ . The full column error bar is the one standard deviation,  $\sigma$ , and the vertical line indicates the minimum and maximum values of  $\varepsilon_{\text{FAPAR}}$ , both obtained by using all the simulations of the training data set. Obviously, the larger the uncertainties of the three spectral bands, the larger the uncertainties in FAPAR: this illustrates the importance of the calibration issues to ensure the quality of the derived product. These results indicate also that the average value,  $\varepsilon_{\text{FAPAR}}$ , can be larger than 10% if two bands have uncertainty values of about 4–5%. The blue band has more impact than the red and near-infrared bands for lower values of uncertainties (e.g.,

$\varepsilon_{\text{FAPAR}} \leq 10\%$  if  $\varepsilon_{\rho\text{BLUE}} \leq 6\%$  with  $\varepsilon_{\rho\text{RED}} = \varepsilon_{\rho\text{NIR}} = 2\%$ ). This result is easily explained by the fact that the blue band is imported twice in the algorithm for removal of the atmospheric effects.

### 3.2. FAPAR differences with respect to sensor band accuracies

This sub-section summarizes the differences between the FAPAR values derived from two sensors with respect to their three respective spectral band accuracies,  $\varepsilon_{\rho\lambda}^S$  where  $\lambda$  correspond to the blue, red and near-infrared bands, respectively. Both FAPAR and spectral accuracy differences derived from two sensors data are defined as follows:

$$\delta_{\text{FAPAR}} = \text{FAPAR}(\varepsilon_{\rho\lambda}^{S1}) - \text{FAPAR}(\varepsilon_{\rho\lambda}^{S2}) \quad (5)$$

$$\delta_{\rho\lambda} = \varepsilon_{\rho\lambda}^{S1} - \varepsilon_{\rho\lambda}^{S2} \quad (6)$$

Note that for one single case of simulation,  $\delta_{\text{FAPAR}}$  varies with respect to  $\delta\rho_\lambda$  for which various couples  $(\varepsilon_{\rho\lambda}^{S1}, \varepsilon_{\rho\lambda}^{S2})$  can occur.

The panels of Fig. 3 display the averaged value,  $\langle\delta_{\text{FAPAR}}\rangle$ , over the ensemble of FAPAR differences,  $\{\delta_{\text{FAPAR}}, i=1,N\}$ , when  $\delta\rho_{\text{BLUE}}$  is equal to  $[-4\%, -2\%, +2\%, +4\%]$  in the spectral space

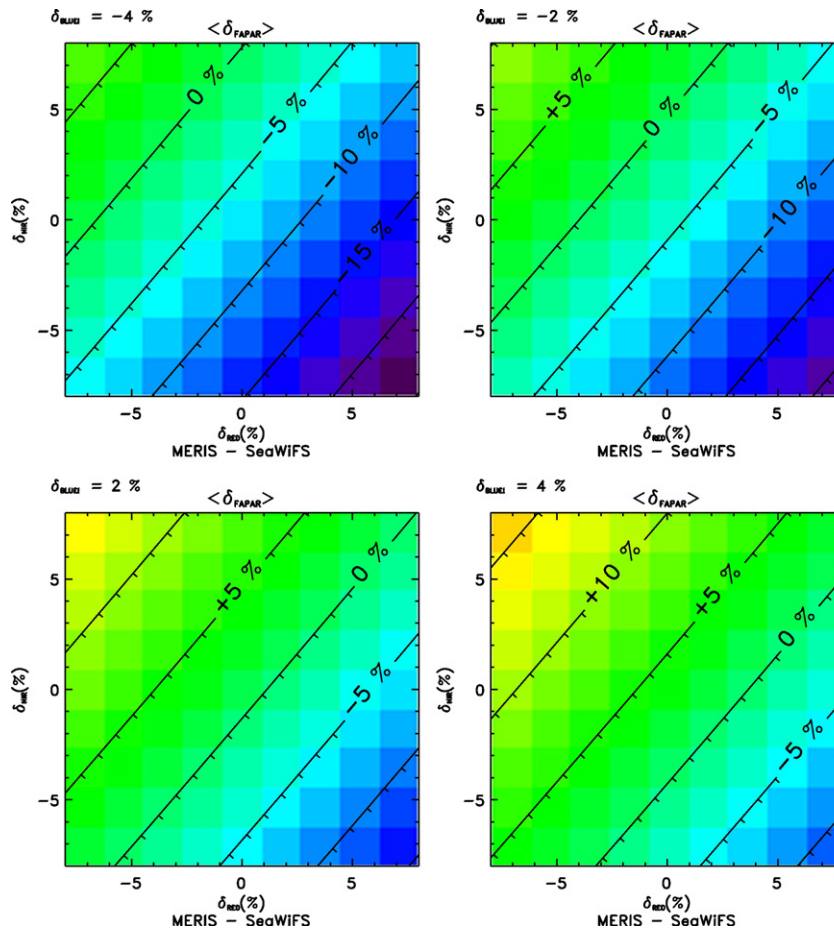


Fig. 3. The 4 panels illustrate the differences of FAPAR,  $\delta_{\text{FAPAR}}$ , between MERIS and SeaWiFS, when the uncertainties difference in the blue band is negative (top panels) or positive (bottom panels). The 4 panels correspond to 4 different values of  $\delta_{\text{BLUE}}$  with respect to the difference of spectral uncertainties in the red and near-infrared bands,  $\delta_{\text{RED}}$  and  $\delta_{\text{NIR}}$ , respectively.

of sensor accuracy differences ( $\delta\rho_{\text{RED}}$ ,  $\delta\rho_{\text{NIR}}$ ). The differences correspond to the MERIS values minus SeaWiFS values, *i.e.*  $S1=\text{MERIS}$  and  $S2=\text{SeaWiFS}$ . In the case  $\delta\rho_{\text{BLUE}}$  has a negative value, the FAPAR values derived from MERIS are smaller than the one derived from SeaWiFS, *i.e.*  $\delta\rho_{\text{FAPAR}} \leq 0$ , except when the MERIS near-infrared band is relatively larger than the SeaWiFS one, simultaneously when the MERIS red band is lower than the SeaWiFS one. An opposite scheme appears when the differences in the blue band between MERIS and SeaWiFS become positive.

Taking the values derived from the calibration and inter-calibration exercises (see Delwart et al., 2003; Kneubuehler et al., 2004; Govaerts & Clerici, 2004 among others), one can expect that the theoretical impact of the spectral band uncertainties on the operational MERIS FAPAR accuracy is in between 5% to 10%. The comparison between simulated products derived from two optical instruments, when using the equivalent FAPAR algorithm, provides the same order of magnitude of variations.

These first analysis and results, for assessing the uncertainties of the operational MERIS FAPAR, can be directly used in any assimilation system by taking into account the propagation errors from the inputs, *i.e.* the spectral measurements. They include both the algorithm and model errors and the instrumental quality of data. The second analysis shows the performance of the algorithm to provide similar FAPAR values and uncertainties when derived from two different sensors.

#### 4. Comparison against ground-based estimations and similar FAPAR products from various sensors

Comparison exercises involving remote sensing products retrieved at low and medium spatial resolutions ( $\approx 1$  km) share a number of issues and face similar caveats that may conflict with each other. First, the uncertainties in the exact location on the Earth geoid of particular pixel coordinates, once re-mapped, may be such that it is advisable to average the fluxes over a cell of  $3 \times 3$  pixels, for instance, to ensure that time series analysis are not performed over a significantly different geophysical system than expected.

On the other hand, the protocols for conducting local ground measurements must be such that they tend to minimize undesirable effects related to the different spatial resolutions between the retrieved remote sensing products and the ground-based measurements. In order to limit the impact of these effects, ground measurements must represent at best the three-dimensional (3-D) spatial variability of the canopy attributes and radiant fluxes existing inside the sampled domain with respect to the sensor pixel resolution.

In the present paper, we are mainly dealing with MERIS derived products re-mapped to a spatial resolution of 1.2 km and SeaWiFS (MODIS) derived products remapped at a spatial resolution of 2.17 (1.1) km, respectively. These spatial resolutions are considered large enough so that the analysis of FAPAR time series can be conducted over the re-mapped pixel identified as the nearest to the nominal location of the measurement site. It also means that the spatial resolution is

slightly too low to fully ensure that the ground-based, eventually domain-averaged, measurements result from a complete spatial sampling at that same spatial resolution (see Turner et al., 2004).

##### 4.1. Ground-based FAPAR data sets

Among ground-based measurements of FAPAR values, there is actually none addressing all in-situ measurements caveats, like the needed vertical and horizontal fluxes separately against the direct and diffuse radiation, measured with the appropriate sampling step and at a spatial resolution compatible with the remote sensing products, for the same ambient conditions as those prevailing during the acquisition of the remote sensing data. Model simulations of realistic vegetation canopy scenarios show that the compensation between different contributions is such that approximating FAPAR by the Fraction of Intercepted Active Radiation (FIPAR) constitutes a first good step in the comparison process (Gobron et al., 2006b; Widlowski et al., 2006).

The following exercise thus relies only on a limited number of proxy data sets that are available over desert grassland, savannah, needle and broadleaf temperate forests. The selected data sets include either or both measurements of local and domain-averaged gap fractions and spatially averaged Leaf Area Index (LAI) and span a wide range of vegetation canopy types which, therefore, can also be roughly categorized according to their expected or most probable RT regimes (as deduced from Davies and Marshak (2004)'s analysis and adapted to the case of vegetation canopies in Gobron et al., 2006b). This helps associating the main RT regimes with the intra-pixel variability of the local leaf extinction density. The three identified RT regimes are summarized as follows: 1) a “fast” variability regime in the case of statistically homogeneous, Poisson-like, distributions of the leaf density, 2) a “slow” variability regime where the leaf density distribution is close enough to being homogeneous only locally such that local scale averaged flux values are meaningful and 3) a “resonant” regime in other cases where the intra-pixel variability controls the domain-averaged flux values.

The latter categorization is based on the qualitative knowledge and description of the field sites and not on the detailed analysis of the leaf density distribution function over the domain as should ideally be done. It seemed appropriate to classify the field sites according to the domain-averaged heights and densities of the prevailing vegetation because these two metrics are inherently linked to their RT regimes and Table 1 lists the various sites and associated references that are used to evaluate the MERIS FAPAR product. A summary of the different approaches adopted to estimate in-situ FAPAR values is also given with detailed characteristics of the field sites and the descriptions of the measuring protocols.

All sorts of combinations of regimes described in Gobron et al. (2006b) coexist at medium and low spatial resolutions. Vegetation canopies are also composed of woody elements for which both statistical and radiative properties significantly differ from those of the green leaves.

Table 1  
Ground-based validation sites: measurement approaches and radiative transfer regime <sup>a</sup>

Field Site Identification	Estimations of the domain-averaged FAPAR	Anticipated radiative regime <sup>b</sup> and land cover type
Dahra <sup>c</sup>	based on BBL's law with measurements of the LAD	1 "Fast variability"
Tessekre <sup>c</sup>	FAPAR( $\mu_0$ ) derived from the balance between the vertical fluxes <LAI> derived from PCA-LICOR	semi-arid grass savannah
Sevilleta <sup>d</sup>	based on BBL's law with an extinction coefficient equal to 0.5 <sup>e</sup> <LAI> derived from optical PCA-LICOR data	1 "Fast variability"
Harvard <sup>d</sup>	Advanced procedure to account for spatio-temporal changes of local LAI based on BBL's law with an extinction coefficient equal to 0.58 <sup>e</sup> <LAI> derived from optical PCA-LICOR data	2 "Slow variability"
Metolius <sup>d</sup>	Advanced procedure to account for spatio-temporal changes of local LAI based on BBL's law with an extinction coefficient equal to 0.5 <sup>e</sup> <LAI> derived from optical PCA-LICOR data	3 "Resonant variability"
	Advanced procedure to account for spatio-temporal changes of local LAI	dry needle-leaf forest

<sup>a</sup> BBL, Beer-Bouguer-Lambert; LAD, Leaf Angle Distribution.

<sup>b</sup> Based on (Davies and Marshak, 2004) analysis.

<sup>c</sup> See (Fensholt et al., 2004).

<sup>d</sup> See (Turner et al., 2004).

<sup>e</sup> Extinction coefficient is taken as constant, *i.e.*, independent of the Sun zenith angle.

#### 4.2. Ground-based comparison results in 2002

Fig. 4 shows the time series of FAPAR products derived from MERIS, SeaWiFS and MODIS together with the ground-based estimations available over the sites geolocated at Dahra North [15° 24' N; 15° 26' W], Tessekre South [15° 49' N; 15° 3' W], Tessekre North [15° 24' N; 15° 26' W] and Sevilleta [34° 2' N; 106° 42' W]. They are associated with RT regime 1 which corresponds to the so-called "fast variability" category.

The ground-based estimations performed at specific dates from July to October 2002 for the three sites located in Senegal and covered by a semi-arid grass savannah, are plotted in green squared symbols, whereas the remote sensing products are over-plotted in red dots for MERIS, blue dots for SeaWiFS and orange dots for MODIS/TERRA. (The zone shaded in light color delineates the  $\pm 0.1$  uncertainty range representing an expected error when comparing remote sensing products to ground-based measurements.) The baseline FAPAR value for all three sites is close to zero and the signatures of the different vegetation phenological cycles (both for the growing and decaying periods) are remarkably well identified by both remote sensing and ground-based estimations. Moreover, the amplitudes, both maxima and minima, are in very good agreement with each other. The ground-based measurements over Sevilleta, corresponding to a desert grassland land cover type, spans from mid-July to the end of November 2002 for a period of 8-days with associated standard deviation represented by the error bars. The FAPAR from the three instruments give the same seasonal variation over this site. However at the end of August, a small decrease appears and this contradicts the ground-based estimations directly derived from the in-situ LAI estimations. It can be due to either a modification in the vegetation spectral properties or to a change in the leaf angle distribution which is not taken into account when using the Beer–Bouguer–Lambert (BBL) law with the assumption of a uniform leaf angle distribution (see Table 1). Interestingly ground-based BigFoot<sup>1</sup>

gross primary productivity estimations show similar patterns to those exhibited by the changes of JRC-FAPAR remote sensing products at the end of August (see Turner et al., 2004, Fig. 5) over this site.

Results over vegetation conditions belonging to the "slow variability" category, that is RT regime 2, are displayed in Fig. 5. The comparison performed with regime 2 canopy conditions, is conducted at the Harvard site [42° 32' N; 72° 10' W] which is a mixture of conifer and hardwood forests. Results from in-situ and remote sensing derived data sets compare very well with each other for the first 6 months of the year that encompass the growing season. The FAPAR products then show systematically lower values (about 0.1) than the ground-based estimations during the summer season when vegetation gets denser over this site. The largest discrepancies are, however, occurring during the senescent period where a time delay of about 1 month is observed from the FAPAR signatures given by the two sources of data sets. This can be explained by the approximation of FAPAR estimates using FIPAR through the BBL which assumes black leaves, *i.e.* fully absorbing leaves, and ignores interception by woody elements whereas the JRC FAPAR algorithm estimates the 'green' absorption. The agreement becomes very good again during the winter season, when the FAPAR values are mostly driven by the relative contribution of the vegetation activity of the coniferous patches (Aber et al., 1996).

The comparison results of ground-based and MERIS retrieved FAPAR over the Metolius site [44° 26' N; 121° 34' W], associated with regime 3 are shown in Fig. 6 with additional retrievals from SeaWiFS and MODIS. The two main interesting features are that 1) both sources of information indicate the absence of a strong seasonal cycle, as could be expected over this young jack pine conifer forest, and 2) the discrepancy in the FAPAR amplitudes between the two data sets is extremely high (about a factor of 2). Interestingly this is a typical class of canopies deviating significantly from the 1-D statistically homogeneous situation. In that instance, the classical BBL law of exponential attenuation can be applied only if the 3-D radiative effects are adequately parameterized (see Pinty et al., 2006a).

<sup>1</sup> <http://www.fsl.orst.edu/larse/bigfoot/index.html>.

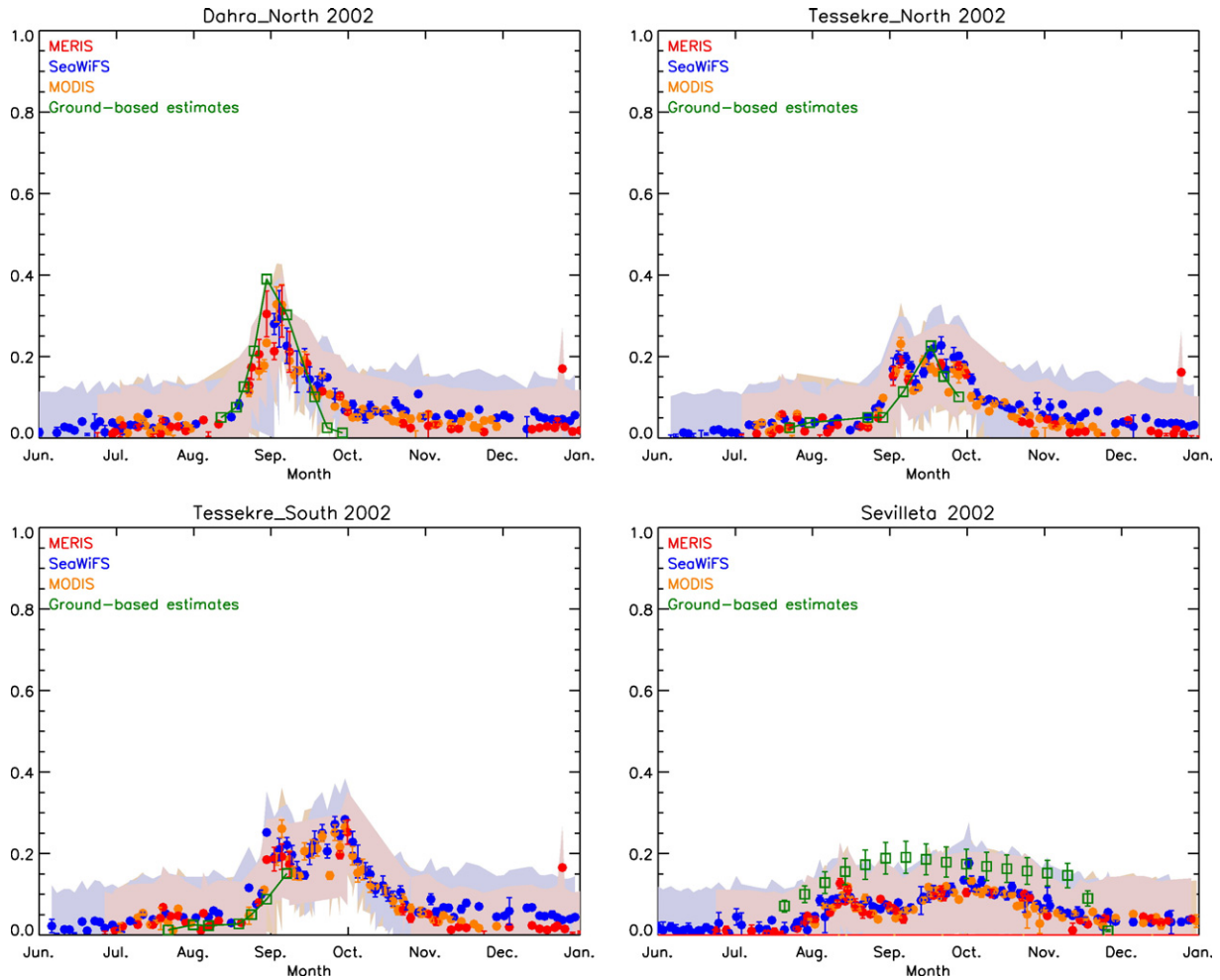


Fig. 4. Comparisons of ground-based FAPAR estimation profiles (empty green square symbols) and instantaneous daily MERIS FAPAR products (red full circle symbols) over the sites of Dahra North [15° 24' N; 15° 26' W]; Tessekre South [15° 49' N; 15° 3' W]; Tessekre North [15° 24' N; 15° 26' W] and Sevilleta [34° 2' N; 106° 42' W] associated with RT regime 1 i.e. for which the 1-D RT theory can be applied on the full domain. The blue and orange dotted points correspond to the SeaWiFS and MODIS derived products, respectively. The light color zones, associated with dots, delineate the  $\pm 0.1$  uncertainty range.

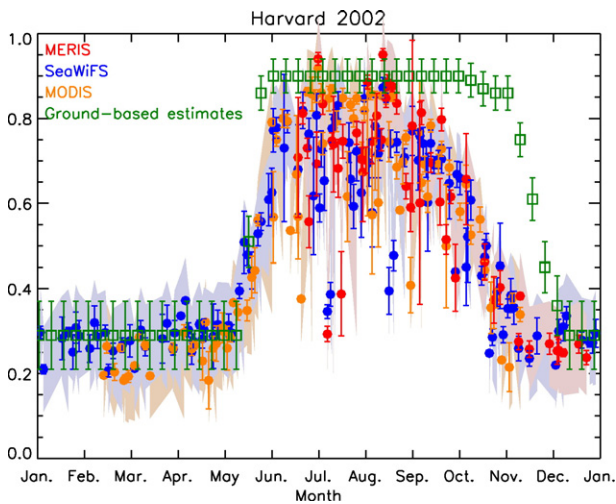
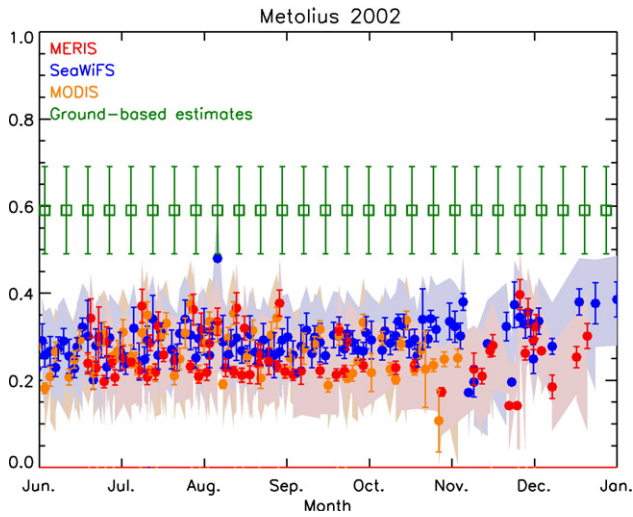


Fig. 5. Same as Fig. 4 except over Harvard site [42° 32' N; 72° 10' W] associated with RT regime 2 i.e. for which the 1-D RT theory can be applied on various land cover types of the domain and over the site.

#### 4.3. Comparisons of JRC FAPAR products derived from different sensors

The performance of the physically-based algorithm of the operational MERIS FAPAR is here assessed through a direct comparison of the actual daily products derived from other optical sensors using the same approach. Three panels in Fig. 7 display scatter-plots of FAPAR derived from a pair of sensors during the year 2002 over the validation sites previously described. The top left panel shows the comparison results between MERIS (x-axis) and SeaWiFS (y-axis). The root mean square values associated with each land cover type vary from 0.0184 (Sevilleta) to 0.096 (Harvard). Note that each dotted point corresponds to the spatially averaged value over  $3 \times 3$  pixels for the exact same day of data acquisition and that values are reported only when at least 5 pixels inside the  $3 \times 3$  pixel domain are associated with a valid FAPAR value.

In general, MERIS and SeaWiFS JRC-FAPAR products agree within  $\approx 0.05$ , MERIS and MODIS JRC-FAPAR products



within  $\approx 0.03$  (bottom left panel) and SeaWiFS and MODIS ones (bottom right panel) within a value of  $\approx 0.04$ . (Note that between two different panels, the ensemble of data points used for the comparison may be derived from different acquisition data). Finally, the top right panel corresponds to the scatter-plot between MERIS and SeaWiFS over the same sites but with data taken in 2003 and with additional validation sites over Braschaat [51° 18' N; 4° 31' E] and Konza prairie [39° 4' N; 96° 33' W]) for which the land cover types are conifer/broad-leaf/shrub forests and grassland/shrub-land/cropland, respectively. These two validation sites, described in Gond et al. (1999) and Turner et al. (2004), respectively, have been already used for JRC-SeaWiFS validation purposes in Gobron et al. (2006b) who associated them with the RT regime 2. This plot shows that the operational FAPAR MERIS is in good agreement with the SeaWiFS products during the entire year of 2003 with an averaged root mean square value equal to  $\approx 0.04$ .

Fig. 6. Same as Fig. 5 except over Metolius site [44° 26' N; 121° 34' W] associated with RT regime 3 i.e. for which the 3-D RT theory should be applied.

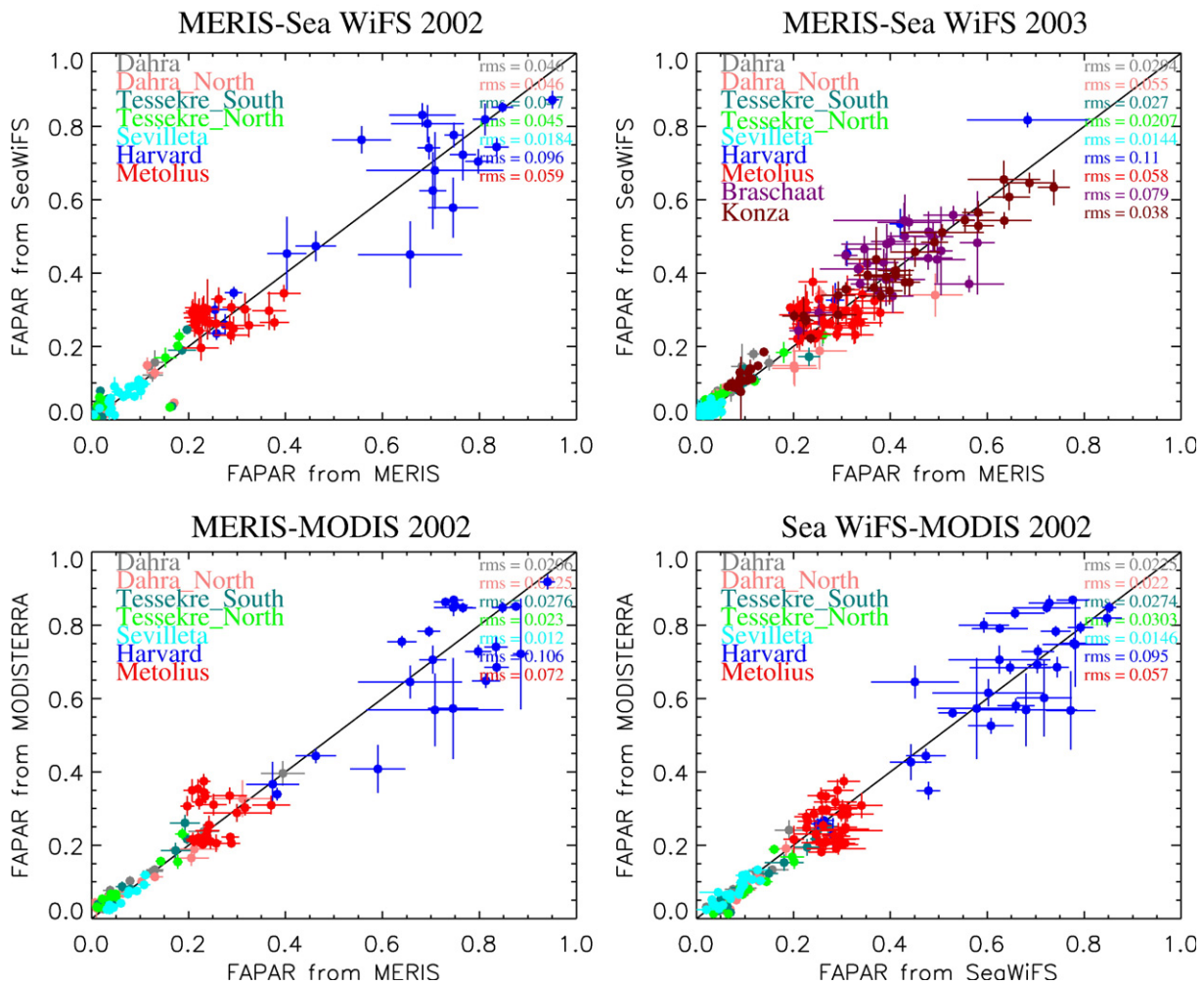


Fig. 7. Top panels: Scatter-plot of the daily FAPAR values derived from MERIS (x-axis) and SeaWiFS (y-axis) over validation sites for 2002 (left) and 2003 (right). Bottom panels: Scatter-plot of the daily FAPAR values derived from MERIS (left) or SeaWiFS (right) (x-axis) and MODIS (y-axis) over validation sites for 2002. The points correspond to the average over a  $3 \times 3$  pixel domain around the central pixel on the common day of acquisition from two sensors. The error bars correspond to the spatial standard deviation around the central pixel.

## 5. Conclusions

This paper presents the results of an evaluation of the quality of the operational MERIS Level 2 land products available since June 2002 at the reduced resolution. This assessment was achieved with the following steps: 1) the theoretical assessment of the FAPAR accuracy with respect to the three input spectral band uncertainties and 2) the inter-comparison with similar FAPAR products associated with a direct comparison against ground-based estimations over sites where field investigations have been carried out at specific periods of time during the mission.

The theoretical accuracy is assessed with respect to spectral band uncertainties. This exercise concludes that the impact of the TOA radiance uncertainties on the expected MERIS FAPAR products accuracy is about 5% to 10%. Moreover, a comparison between FAPAR products from different sensors show differences in the range 5–10% when the inter-calibration uncertainty between spectral bands are lower than 4%. Given the number of complex theoretical and technical issues and caveats to be faced, the current comparison exercise against ground-based estimations capitalizes on the limited but available in-situ measurements over various land cover types and during full seasonal cycles. A categorization of the different sites where FAPAR field data sets are available, based on the anticipated RT regimes, was used to better identify and thus recognize the level of difficulties to be faced for achieving such comparisons against in-situ estimations.

Overall, the comparison results are encouraging since the MERIS FAPAR products behave as can be expected given the difficulties associated with each RT regime mentioned above. The FAPAR products notably display a quite good representation of the seasonal cycles as can be inferred from ground-based estimations, e.g. for the evaluated environmental conditions. The JRC- FAPAR products, corresponding to the green contribution, may be lower than the in-situ measurements during senescence period over some vegetation types because during this phase the LAI decreases and the leaf color changes which is not taken into account when ground-based estimates are approximated by the BBL.

In the context of building long term time series of biophysical products based on the merging of products from a panoply of sensors, the performance of the JRC FAPAR algorithm was assessed using three contemporaneous optical sensors operating at medium spatial resolution. Additional validation exercises should continue during the life time of the MERIS sensor in order to assess the quality of the operational products while more efforts should be devoted to higher spatial resolution using the full resolution MERIS data sets.

The BEAM “MERIS FAPAR Processor” is available at <http://www.brockmann-consult.de/beam/plugins.html>. The JRC-FAPAR products derived from SeaWiFS are available at the following address: <http://fapar.jrc.ec.europa.eu/>.

## Acknowledgments

This work has been supported by the ESTEC Contract 18446/04/NL/CB and has been possible with the financial support of

the European Commission, and more specifically, the Global Environment Monitoring unit of the Institute for Environment and Sustainability in the DG Joint Research Centre.

The MERIS FAPAR products are available at <http://earth.esa.int/> from the European Space Agency (ESA).

The authors thank R. Fensholt and I. Sandholt (Institute of Geography, University of Copenhagen), W. B. Cohen (USDA Forest Service) and D. P. Turner (Oregon State University) for providing the ground-based estimates over the Senegal and Bigfoot (*i.e.* Sevilleta, Harvard and Metolius) sites, respectively.

The authors are grateful to the SeaWiFS Project (Code 970.2) and the Distributed Active Archive Center (Code 902) at the Goddard Space Flight Center, Greenbelt, MD 20771, for the production and distribution of the SeaWiFS data, respectively.

The MODIS data used in this study were acquired as part of the NASA’s Earth–Sun System Division and archived and distributed by the Goddard Earth Sciences (GES) Data and Information Services Center (DISC) Distributed Active Archive Center (DAAC).

## Appendix A

The following equations correspond to the derivative formulae used in the assessment of the theoretical accuracy of the FAPAR algorithm.

The mathematical formula to evaluate the derivative of  $g_0$ , (polynomial formula to compute the FAPAR from the two rectified channels) with respect to the rectified red channel,  $\rho_{\text{RectRed}}$ , is given by Eq. (7):

$$\frac{\partial g_0}{\partial \rho_{\text{RectRed}}} = \frac{2(l_{04} - \rho_{\text{RectRed}})(-l_{02}\rho_{\text{RectRed}} + l_{01}\rho_{\text{RectNIR}} - l_{03})}{\left((l_{04} - \rho_{\text{RectRed}})^2 + (l_{05} - \rho_{\text{RectNIR}})^2 + l_{06}\right)^2} - \frac{l_{02}}{(l_{04} - \rho_{\text{RectRed}})^2 + (l_{05} - \rho_{\text{RectNIR}})^2 + l_{06}} \quad (7)$$

and the mathematical formula to evaluate the derivative of  $g_0$  with respect to the rectified NIR channel,  $\rho_{\text{RectNIR}}$ , by Eq. (8).

$$\frac{\partial g_0}{\partial \rho_{\text{RectNIR}}} = \frac{2(l_{05} - \rho_{\text{RectNIR}})(-l_{02}\rho_{\text{RectRed}} + l_{01}\rho_{\text{RectNIR}} - l_{03})}{\left((l_{04} - \rho_{\text{RectRed}})^2 + (l_{05} - \rho_{\text{RectNIR}})^2 + l_{06}\right)^2} - \frac{l_{01}}{(l_{04} - \rho_{\text{RectRed}})^2 + (l_{05} - \rho_{\text{RectNIR}})^2 + l_{06}} \quad (8)$$

where the coefficients  $l_{0j}$  correspond to the optimized parameters to fit the FAPAR values. The most recent versions are given in Gobron et al. (2002) for SeaWiFS, Gobron et al. (2007) for MERIS, and Gobron et al. (2006a) for MODIS, respectively.

The derivatives of  $g_n$  (where  $g_n$  denotes  $g_1$  ( $g_2$ ) and corresponds to the polynomial formulae to compute the rectified channel in the red (near-infrared)) with respect to the blue band,  $\rho_1$ , and with respect to the red (near-infrared) band,  $\rho_2$ , are given by the Eqs. (9) and (10), respectively.

Both polynomial expressions  $g_n$  and associated coefficients  $l_{nj}$  were optimized to give equivalent values of normalized

reflectances at the top-of-canopy.  $\rho_\lambda$  used in these equations are the TOA BRFs normalized by the anisotropical function of the RPV model (Rahman et al., 1993).

$$\frac{\partial g_n}{\partial \rho_1} = \frac{\rho_2 I_{n5} + 2I_{n1}(I_{n2} + \rho_1)}{I_{n8}(I_{n9} + \rho_2)^2 + I_{n6}(I_{n7} + \rho_1)^2 + I_{n11} + \rho_1 \rho_2 I_{n10}} - \frac{(\rho_1 \rho_2 I_{n5} + I_{n3}(I_{n4} + \rho_2)^2 + I_{n1}(I_{n2} + \rho_1)^2)(2I_{n6}(I_{n7} + \rho_1) + \rho_2 I_{n10})}{(I_{n8}(I_{n9} + \rho_2)^2 + I_{n6}(I_{n7} + \rho_1)^2 + I_{n11} + \rho_1 \rho_2 I_{n10})^2} \quad (9)$$

$$\frac{\partial g_n}{\partial \rho_2} = \frac{\rho_1 I_{n5} + 2I_{n3}(I_{n4} + \rho_2)}{I_{n8}(I_{n9} + \rho_2)^2 + I_{n6}(I_{n7} + \rho_1)^2 + I_{n11} + \rho_1 \rho_2 I_{n10}} - \frac{(\rho_1 \rho_2 I_{n5} + I_{n3}(I_{n4} + \rho_2)^2 + I_{n1}(I_{n2} + \rho_1)^2)(2I_{n8}(I_{n9} + \rho_2) + \rho_1 I_{n10})}{(I_{n8}(I_{n9} + \rho_2)^2 + I_{n6}(I_{n7} + \rho_1)^2 + I_{n11} + \rho_1 \rho_2 I_{n10})^2} \quad (10)$$

In Eqs. (7)–(10), the notation  $I_{nj}$  corresponds to the coefficients in their intrinsic polynomial expression. The most recent versions are given in Gobron et al. (2002) for SeaWiFS, Gobron et al. (2007) for MERIS, and Gobron et al. (2006a) for MODIS, respectively.

## References

- Aber, J. D., Reich, P. B., & Goulden, M. L. (1996). Extrapolating leaf CO<sub>2</sub> exchange to the canopy: A generalized model of forest photosynthesis validated by eddy correlation. *Oecologia*, 106, 267–275.
- Bourg, L., & Obelensky, G. (2006). Evolution of the MERIS instrument processing facility. *Technical Note April 2006*: ESA.
- Davies, A. B., & Marshak, A. (2004). Photon propagation in heterogeneous optical media with spatial correlations: Enhanced mean free-paths and wider-than-exponential free-path distributions. *Journal of Quantitative Spectroscopy & Radiative Transfer*, 84, 3–34.
- Delwart, S., Bourg, L., & Huot, J. (2003). MERIS 1st year: Early calibration results. In R. Meynart, S. P. Neeck, H. Shimoda, J. B. Lurie, & M. L. Aten (Eds.), *Sensors, Systems, and Next-Generation Satellites VII* (pp. 614–623).
- Fensholt, R., Sandholt, I., & Rasmussen, M. S. (2004). Evaluation of MODIS LAI, fAPAR and the relation between fAPAR and NDVI in a semi-arid environment using in situ measurements. *Remote Sensing of Environment*, 91, 490–507.
- GCOS. (2004). Implementation Plan for the Global Observing System for Climate in Support of the UNFCCC. *October, 2004 GCOS-92*: World Meteorological Organization.
- Gobron, N., Pinty, B., Verstraete, M. M., & Govaerts, Y. (1997). A semi-discrete model for the scattering of light by vegetation. *Journal of Geophysical Research*, 102, 9431–9446.
- Gobron, N., Pinty, B., Verstraete, M. M., & Govaerts, Y. (1999). The MERIS Global Vegetation Index (MGVI): description and preliminary application. *International Journal of Remote Sensing*, 20, 1917–1927.
- Gobron, N., Pinty, B., Verstraete, M. M., & Widlowski, J. L. (2000). Advanced spectral algorithm and new vegetation indices optimized for up coming sensors: Development, accuracy and applications. *IEEE Transactions on Geoscience and Remote Sensing*, 38, 2489–2505.
- Gobron, N., Mélin, F., Pinty, B., Verstraete, M. M., Widlowski, J. L., & Bucini, G. (2001). A global vegetation index for SeaWiFS: Design and applications. In M. Beniston & M. M. Verstraete (Eds.), *Remote Sensing and Climate Modeling: Synergies and Limitations* (pp. 5–21). Dordrecht, The Netherlands: Kluwer Academic Publishers.
- Gobron, N., Pinty, B., Mélin, F., Taberner, M., & Verstraete, M. M. (2002). Sea Wide Field-of-View Sensor (SeaWiFS) – Level 2 land surface products – Algorithm Theoretical Basis Document. *EUR Report No. 20144 EN*: Institute for Environment and Sustainability.
- Gobron, N., Pinty, B., Mélin, F., Taberner, M., Verstraete, M. M., Belward, A., Lavergne, T., & Widlowski, J. L. (2005a). The state of vegetation in Europe following the 2003 drought. *International Journal Remote Sensing Letters*, 26(9), 2013–2020.
- Gobron, N., Verstraete, M. M., Pinty, B., Aussedat, O., & Taberner, M. (2005b). Potential of long time series of FAPAR products for assessing and monitoring land surfaces changes. *Remote Sensing and Geoinformation Processing in the Assessment and Monitoring of Land Degradation and Desertification, State of the Art and Operational Perspectives, 7–9 September 2005*: Achim Roder and Joachim Hill.
- Gobron, N., Aussedat, O., & Pinty, B. (2006a). MODerate Resolution Imaging Spectroradiometer, JRC-FAPAR Algorithm Theoretical Basis Document. *EUR Report No. 22164 EN*: Institute for Environment and Sustainability.
- Gobron, N., Pinty, B., Aussedat, O., Chen, J. M., Cohen, W. B., Fensholt, R., Gond, V., Huemmrich, K. F., Lavergne, T., Mélin, F., Privette, J. L., Sandholt, I., Taberner, M., Turner, D. P., Verstraete, M., & Widlowski, J. L. (2006b). Evaluation of FAPAR products for different canopy radiation transfer regimes: Methodology and results using jrc products derived from SeaWiFS against ground-based estimations. *Journal of Geophysical Research*, 111, D13110. doi:10.1029/2005JD006511
- Gobron, N., Pinty, B., Mélin, F., Taberner, M., Verstraete, M., Robustelli, M., & Widlowski, J. L. (2007). Evaluation of the MERIS/ENVISAT FAPAR product. *Advances in Space Research*, 39, 105–115. doi:10.1016/j.asr.2006.02.048
- Gond, V., de Pury, D. G. G., Veroustraete, F., & Ceulemans, R. (1999). Seasonal variations in leaf area index, leaf chlorophyll, and water content; scaling-up to estimate FAPAR and carbon balance in a multilayer, multispecies temperate forest. *Tree Physiology*, 19, 673–679.
- GOOS. (2006). IOC-WMO-UNEP-ICSU scientific steering committee of the global ocean observing system (GOOS). *January, 2006 GOOS-151*: UNESCO.
- Govaerts, Y., Verstraete, M. M., Pinty, B., & Gobron, N. (1999). Designing optimal spectral indices: A feasibility and proof of concept study. *International Journal of Remote Sensing*, 20, 1853–1873.
- Govaerts, Y., Lattanzio, A., Pinty, B., & Schmetz, J. (2004). Consistent surface albedo retrieval from two adjacent geostationary satellites. *Geophysical Research Letters*, 31, L15,201. doi:10.1029/2004GL020418
- Govaerts, Y. M., & Clerici, M. (2004). Evaluation of radiative transfer simulations over bright desert calibration sites. *IEEE Transactions on Geoscience and Remote Sensing*, 42, 176–187.
- GTOS. (2006). Global terrestrial observation system biennial report 2004–2005. *January, 2006 GTOS-40*: FAO.
- Hall, F., Masek, J. G., & Collatz, G. J. (2006). Evaluation of ISLSCP Initiative II FASIR and GIMMS NDVI products and implications for carbon cycle science. *Journal of Geophysical Research*, 111, D22,808. doi:10.1029/2006JD007438
- Isaacman, A., Toller, G., Guenther, B., Barnes, W. L., & Xiong, X. (2003). MODIS Level 1B calibration and data products. *SPIE, Earth Observation Systems VIII, 5151*, 552–562.
- Kneubuehler, M., Schaepman, M. E., Thome, K. J., & Schlapfer, D. R. (2004). MERIS/ENVISAT vicarious calibration over land. In R. Meynart, S. P. Neeck, H. Shimoda, J. B. Lurie, & M. L. Aten (Eds.), *Sensors, Systems, and Next-Generation Satellites VII*. Edited by Meynart, Roland; Neeck, Steven P.; Shimoda, Haruhisa; Lurie, Joan B.; Aten, Michelle L. *Proceedings of the SPIE, vol. 5234* (pp. 614–623). doi:10.1117/12.510449
- Knorr, W., & Heimann, M. (1995a). Impact of drought stress and other factors on seasonal land biosphere CO<sub>2</sub> exchange studied through an atmospheric tracer transport model. *Tellus*, 47B, 471–489.
- Knorr, W., Gobron, N., Martin, P., Pinty, B., Verstraete, M. M., & Dedieu, G. (1995b). Constraining a climate driven vegetation model with satellite data. In G. Guyot (Ed.), *Proceedings of the International Colloquium on Photosynthesis and Remote Sensing, Montpellier, 28–30 August 1995* (pp. 269–279). EARSeL.
- Knorr, W., Gobron, N., Scholze, M., Kaminski, T., & Pinty, B. (2005a). Global drought conditions causing recent atmospheric carbon dioxide increase. *EOS, Transactions — American Geophysical Union*, 86, 178–181.
- Knorr, W., Gobron, N., Scholze, M., Rayner, P., Kaminski, T., Giering, R., Widman, H., & Kattge, J. (2005b). Carbon and FAPAR assimilation within CCDAS. In P. Viterbo (Ed.), *Proceedings of ECMWF/ELDAS Workshop on Land Surface Assimilation 8–11 November 2004* (pp. 213–219). European Centre for Medium Range Weather Forecasts.

- Maritorena, S., & Siegel, D. A. (2005). Consistent merging of satellite ocean color data sets using a bio-optical model. *Remote Sensing of Environment*, 94, 429–440.
- Mélin, F., & Zibordi, G. (2007). An optically-based technique for producing merged spectra of water leaving radiances from ocean color. *Applied Optics*, 46, 3856–3869.
- Mélin, F., Steinich, C., Gobron, N., Pinty, B., & Verstraete, M. (2002). Optimal merging of LAC and GAC data from SeaWiFS. *International Journal of Remote Sensing*, 23, 801–807.
- Pinty, B., Lavergne, T., Dickinson, R. E., Widlowski, J. L., Gobron, N., & Verstraete, M. M. (2006a). Simplifying the interaction of land surfaces with radiation for relating remote sensing products to climate models. *Journal of Geophysical Research*, 111, D02116. doi:10.1029/2005JD005952
- Pinty, B., Lavergne, T., Vossbeck, M., Kaminski, T., Aussedat, O., Giering, R., Gobron, N., Taberner, M., Verstraete, M., & Widlowski, J. L. (2006b). Retrieving surface parameters for climate models from MODIS-MISR albedo products. *Journal of Geophysical Research*, 112. doi:10.1029/2006JD008105
- Prince, S. D. (1991). A model of regional primary production for use with coarse resolution satellite data. *International Journal of Remote Sensing*, 12, 1313–1330.
- Rahman, H., Verstraete, M. M., & Pinty, B. (1993). Coupled surface-atmosphere reflectance (CSAR) model. 1. Model description and inversion on synthetic data. *Journal of Geophysical Research*, 98, 20,779–20,789.
- Raupach, M. R., Rayner, P., Barrett, D., DeFries, R., Heimann, M., Ojima, D., Quegan, S., & Schimmlius, C. (2005). Model-data synthesis in terrestrial carbon observation: methods, data requirements and data uncertainty specifications. *Global Change Biology*, 11(3), 378–397. doi:10.1111/j.1365-2486.2005.00917.x
- Rayner, P., Scholze, M., Knorr, W., Kaminski, R., Giering, R., & Widmann, H. (2005). Two decades of terrestrial carbon fluxes from a carbon cycle data assimilation system CCDAS. *Global Biogeochemical Cycles*, 10. doi:10.1029/2004GB002254
- Reynolds, R. W., & Smith, T. M. (1994). Improved global sea surface temperature analyses. *Journal of Climate*, 7, 929–948.
- Running, S. (1986). Global primary production from terrestrial vegetation: Estimates integrating satellite remote sensing and computer simulation technology. *Science of The Total Environment*, 56, 233–242.
- Seiler, R., & Csaplovics, E. (2005). Monitoring dynamics of land cover in semi-arid wetlands. A case study for the Niger inland delta (Mali). *Remote Sensing and Geoinformation Processing in the Assessment and Monitoring of Land Degradation and Desertification, State of the Art and Operational Perspectives, 7–9 September 2005* (pp. 556–562). Achim Roder and Joachim Hill.
- Sellers, P. J., Berry, J. A., Collatz, G. J., Field, C. B., & Hall, F. (1992). Canopy reflectance, photosynthesis, and transpiration. III A reanalysis using improved leaf models and a new canopy integration scheme. *Remote Sensing of Environment*, 42, 187–216.
- Turner, D. P., Ritts, W. D., Cohen, W. B., Maeirsperger, T., Gower, S. T., Kirschbaum, A., Running, S. W., Zhao, M., Wofsy, S., Dunn, B., Law, A., Campbell, J., Oechel, W., Kwon, H. J., Meyers, T., Small, E., Kurc, S., & Gamon, J. (2004). Site-level evaluation of satellite-based global terrestrial GPP and NPP modeling. *Global Change Biology*, 11, 666–684. doi:10.1111/j.1365-2486.2005.00936.x
- Vermote, E., Tanré, D., Deuzé, J. L., Herman, M., & Morcrette, J. J. (1997). Second simulation of the satellite signal in the solar spectrum: An overview. *IEEE Transactions on Geoscience and Remote Sensing*, 35–3, 675–686.
- Verstraete, M. M., Gobron, N., Aussedat, O., Pinty, B., Robustelli, M., Taberner, M., Lavergne, T., & Widlowski, J. L. (2007). Objectively determining the start and end of growing seasons on the basis of remote sensing FAPAR products. *Advances in Space Research*. doi:10.1016/j.asr.2007.05.066 (In print).
- Widlowski, J. L., Pinty, B., Lavergne, T., Verstraete, M. M., & Gobron, N. (2006). Horizontal radiation transport in 3-d forest canopies at multiple spatial resolutions: Simulated impact on canopy absorption. *Remote Sensing of Environment*, 103, 379–397. doi:10.1016/j.rse.2006.03.014